ISSN 0036-0244, Russian Journal of Physical Chemistry A, 2023, Vol. 97, No. 6, pp. 1232–1238. © Pleiades Publishing, Ltd., 2023.

PHYSICAL CHEMISTRY OF NANOCLUSTERS, SUPRAMOLECULAR STRUCTURES, AND NANOMATERIALS

Hydrothermal Synthesis and Photocatalytic Activity of Layered Perovskite-Like Titanate $K_2La_2Ti_3O_{10}$ Ultrafine Nanoplatelets

I. Minich[a,b], S. Kurnosenko[a], O. Silyukov[a], I. Rodionov[a], V. Kalganov[c], and I. Zvereva[a,*]

[a] *Institute of Chemistry, St. Petersburg State University, St. Petersburg, 199034 Russia*

[b] *Centre for Thermal Analysis and Calorimetry, St. Petersburg State University, St. Petersburg, 199034 Russia*

[c] *Interdisciplinary Centre for Nanotechnology, St. Petersburg State University, St. Petersburg, 199034 Russia*

** e-mail: irina.zvereva@spbu.ru*

Received December 1, 2022; revised December 1, 2022; accepted December 16, 2022

Abstract—Layered perovskite-like oxide $K_2La_2Ti_3O_{10}$ belonging to Ruddlesden-Popper phases was prepared by hydrothermal method from commercially available precursors. Various conditions, namely reaction time, temperature and precursors concentration were varied to prepare well-crystallized single phase product. Morphology, specific surface area, band gap and photocatalytic activity in reaction of hydrogen evolution from methanol water solution had been investigated in comparison with oxide prepared by conventional ceramic method. Hydrothermally prepared oxide has an ultrafine plate-like morphology with 4–5 nm particles thickness and relatively big lateral sizes of about 2–5 μm. Obtained samples have ~10 times higher specific surface area and ~3 times higher photocatalytic activity comparing to the ceramic sample, however using Pt co-catalysts leads to the lower photocatalytic activity of hydrothermal sample comparing to ceramic one. Developed approach may be further used for preparation of organic-inorganic hybrids and monolayers based on $H_2La_2Ti_3O_{10}$ for further enhancement of photocatalytic activity.

Keywords: layered perovskite, titanate, hydrothermal synthesis, nanoplatelets, photocatalysis, hydrogen production

DOI: 10.1134/S0036024423060079

1. INTRODUCTION

Recently ion-exchangeable layered perovskite-like oxides have attracted a special attention as promising high performance photocatalysts in the reactions of hydrogen production due to their possibility to intercalate water molecules into the interlayer space. One of the most studied Ruddlesden-Popper phases for catalytic applications is $K_2La_2Ti_3O_{10}$, which was shown to exhibit high photocatalytic activity both in an alkali form and after various modifications including the use of co-catalysts and sensitizers and creation of heterostructured photocatalysts [1–6]. Recently, we have shown the efficiency of organic modification of $H_2La_2Ti_3O_{10}$ and $HCa_2Nb_3O_{10}$ with a row of *n*-amines and *n*-alcohols for the preparation of new hybrid organic-inorganic photocatalysts providing enhanced quantum yields in the reactions of hydrogen generation [7–10]. Upon the organic modification the photocatalytic activity was shown to increase up to 100 times. Another important property of layered oxides is their possibility to be exfoliated along the interlayer space [11–16]. This process is often used for protonated and organic-inorganic derivatives as a possible approach to obtain nanoplatelets with perovskite structure, which possesses higher specific surface area comparing to the starting compound, prepared by the solid-state reaction. Obtained nanoplatelets are considered to demonstrate higher catalytic activity; however, this approach considers application of ion-exchanged forms without alkali cations in the interlayer space, which may have a negative or in single cases positive impact on the photocatalytic activity [4, 17–19]. Another negative factor affecting the activity may be the formation of disorders and defects in morphology and structure of the nanoplatelets, as a result of a sequence of soft chemistry reactions and exfoliation [20]. In addition, it seems reasonable to use powders with originally finer morphologies for further modification. Hydrothermal and sol-gel syntheses are known as effective methods to prepare ceramics with desired morphologies and surface area for catalysis, photocatalysis, anode materials and etc. [6, 21–26]. In case of photocatalysis, hydrothermal synthesis is preferable towards sol-gel synthesis as it provides higher crystallinity of resulted materials. Hydrothermal synthesis is widely presented in literature for a number of 3D perovskite oxides, layered hydroxides [27], however only a couple of works shows attempts to prepare layered ion-exchangeable perovskite-like oxides by this method. To our knowledge, such procedures are shown for two well-known layered phases, namely

Ruddlesden-Popper phase $K_2La_2Ti_3O_{10}$ [28] and Dion-Jacobson phase $KCa_2Nb_3O_{10}$ [29]. In [29] the formation of the pure phase $KCa_2Nb_3O_{10}$ was reported, however authors were forced to resort to post-heating of the sample at relatively high temperature, which did not allow them to obtain ultrafine powders as planned. In [28] authors suggest the preparation of $K_2La_2Ti_3O_{10}$ by pure hydrothermal procedure at quite mild conditions (180–280°C, 12–72 h). The formation of the desired phase is proved by XRD analysis and higher specific surface area and photocatalytic activity were shown for the hydrothermally obtained samples comparing to the ceramically synthesized sample. However, the results suggest that the morphology and crystallinity of the sample do not show any significant benefits comparing to sol-gel synthesis and, moreover, the formation of the pure phase was not possible in tested conditions. Therefore, in the present work, we repeated an attempt to optimize reaction conditions and to obtain pure-phase samples of $K_2La_2Ti_3O_{10}$ with high crystallinity and fine plate-like morphology. In our work we relied on previously reported data, however the procedure and studied conditions had been changed along with the Ti-containing precursor. For comparison, $K_2La_2Ti_3O_{10}$ was also synthesized by the conventional ceramic procedure.

2. MATERIALS AND METHODS

2.1. Ceramic Synthesis of $K_2La_2Ti_3O_{10}$

Conventional ceramic synthesis of $K_2La_2Ti_3O_{10}$ was carried out in the air atmosphere at atmospheric pressure, using La_2O_3 (99.9%, Vekton), TiO_2 (99.9%, Vekton) and K_2CO_3 (99.8%, Vekton), which were preliminarily calcined at 600, 900, and 200°C, correspondingly, to remove traces of moisture.

Amounts of oxides La_2O_3 and TiO_2 were taken according to stoichiometry of the reaction:

$$La_2O_3 + 3TiO_2 + K_2CO_3 = K_2La_2Ti_3O_{10} + CO_2\uparrow.$$

Potassium carbonate K_2CO_3 was taken with a 30% excess to compensate for its loss due to volatilization during calcination. All the reactants were mixed, placed into a grinding bowl with silicon nitride balls, flooded with *n*-heptane and ground in a Fritsch Pulverisette 7 planetary micro mill at a speed of 600 rpm using a program of 10 repetitions of 10 min each with 5 min intervals. The mixture obtained was dried and pressed into ~2 g tablets at 50 bar using an Omec PI 88.00 hydraulic press. The tablets were placed into corundum crucibles with lids and heated at 1100°C for 15 h in a Nabertherm L-011K2RN muffle furnace twice. After the first calcination the tablets were ground, mixed and pressed again.

2.2. Hydrothermal Synthesis of $K_2La_2Ti_3O_{10}$

In case of hydrothermal synthesis, the starting materials were La_2O_3 (Vekton, 99.9%), TiO_2 (Evonik Aeroxide P25), and KOH (Vekton, 99.9%) as both precursor and the reaction medium. It should be underlined, that in the case of hydrothermal synthesis no preliminary calcination of the precursors was performed and the amounts were taken according to the mass loss on TG curves (Netzsch TG 209 F1 Libra) due to the water desorption. La_2O_3 and TiO_2 calcination could lead to its agglomeration and, therefore, lower dispersibility in the reaction medium and reactivity.

The typical synthesis procedure may be described as follows. The stoichiometric amounts of TiO_2 and La_2O_3 calculated for 250 mg (in some cases 125 and 500 mg) of the product were weighed and suspended in 40 mL of KOH water solution. The suspension was sonicated in a closed round-bottom flask for 15 min and placed in a 50 mL Teflon-lined vessel. The vessel was then inserted into a stainless steel autoclave and heated at desired temperature in a digital drying oven with thermocouple temperature control. After the reaction, the vessel was naturally cooled in the air for ~3 h and the precipitate was separated by centrifugation. The obtained slurry material was washed once with 40 mL of distilled water and twice with 40 mL of ethanol and dried in air overnight in order to avoid the protonation of the sample.

2.3. Characterization of the Products

Powder X-ray diffraction (XRD) patterns of the products were obtained on a Rigaku Miniflex II benchtop diffractometer (CuK_α radiation, angle range 1 $2\theta = 3°–60°$, scanning rate 10°/min, step 0.02°). The lattice parameters in the tetragonal system and crystallite sizes were calculated on the basis of all the reflections observed using DiffracPlus Topas software.

Diffuse reflectance spectra (DRS) were recorded on a Shimadzu UV-2550 spectrophotometer with an ISR-2200 integrating sphere using barium sulfate BaSO4 as an external standard with reflection coefficient $R = 1$. Optical bandgap energies E_g were found via transformation of reflectance spectra into coordinates $(Fh\nu)^{1/2} = f(h\nu)$, where $F = (1 - R)^2/2R$ is the Kubelka–Munk function, and further determination of abscissas of the intersection points of linear sections of the graphs.

Morphology of the particles was investigated on a Zeiss Merlin scanning electron microscope (SEM) with a field emission cathode, an electron optics column GEMINI-II and an oil-free vacuum system.

Specific surface areas S were measured according to the Brunauer–Emmett–Teller (BET) method on a Micromeritics ASAP 2020MP system with previous vacuum degassing at 150°C using N_2 and Kr as adsorp-

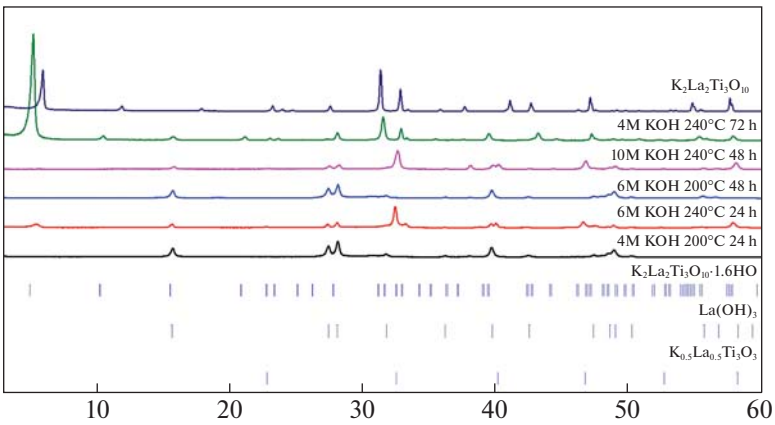

Fig. 1. XRD patterns of the samples obtained in various reaction conditions.

tives (for the samples obtained by ceramic and hydrothermal methods correspondingly).

2.4. Study of Photocatalytic Activity

Photocatalytic activity of the products was investigated in the reaction of light-driven hydrogen evolution from the model 1% (mol) aqueous solution of methanol both for bare samples and for their composites with 1% (mass) Pt as a co-catalyst. The program of photocatalytic experiments additionally included dark stages as well as determination of pH and bulk concentrations of the samples in suspensions at the beginning of the photocatalytic experiment (pH_1, c_1), in the ending (pH_2, c_2) and after centrifuging of the suspension at 1000 RCF for 1 h (pH_3, c_3) to take into account possible changes of the suspension concentration during the experiment and potential exfoliation of the samples into nanolayers. The hydrogen generation rate ω, apparent quantum efficiency φ and multiplicity kPt of increase in the rate after Pt loading were used as quantitative indicators of photocatalytic activity. Detailed information on the photocatalytic equipment, methodologies for the measurement of photocatalytic activity, pH values and concentrations of the suspensions as well as the obtained data processing was presented in our previous works [7, 9].

3. RESULTS AND DISCUSSION

3.1. Synthesis

Optimization of reaction conditions was performed based on previously reported data where titanium (IV) isopropoxide was used as a Ti-containing precursor. The authors suggested that the optimal reaction temperature was 200°C and reaction time – 24 h using 4 M KOH, however the XRD data for various reaction times at 200°C with 4M KOH demonstrated no layered phases present in the sample after 24 h and $K_2La_2Ti_3O_{10}$ formation may be detected on XRD patterns only after 48–72 h of the reaction time. Therefore, we started with the conditions, considered optimal by the previous authors, and then varied some parameters (alkali concentration, time, precursors concentration and, in some cases, temperature).

Figure 1 shows XRD patterns of the samples obtained in various reaction conditions (temperature, time and KOH concentration). As shown, the reaction at 200°C for 24 h using 4 M KOH did not yield in the aimed layered Ruddlesden-Popper titanate and only formation of amorphous phases and $La(OH)_3$ is observed (ICDD card no. 01-077-3933). Raising the KOH concentration up to 6M and temperature up to 240°C resulted in the formation of $La_{0.5}K_{0.5}TiO_3$ 3D perovskite (ICDD card no. 01-089-4930) additionally to the $La(OH)_3$, also some reflections that could belong to the layered phase appeared. In order to suppress the formation of non-layered phase, we decided to lower reaction temperature back to 200°C (using 6M KOH) and increase the reaction time up to 48 h. These reaction conditions did not yield aimed compound but $La(OH)_3$. Further increase in KOH concentration (10 M) at 240°C leads to the formation of stable $La_{0.5}K_{0.5}TiO_3$ phase with impurity of $La(OH)_3$, but decrease of KOH concentration (4 M) finally led to the formation of pure-phase $K_2La_2Ti_3O_{10}$ at 240°C heating for 72 h.

The results for the product of the optimized synthetic procedure show the formation of a well crystallized single phase. The diffraction peaks are slightly broadened compared to the samples, obtained by conventional high-temperature ceramic technique [30], which indicates the decrease in the crystallite size. All of the diffraction peaks correspond to the hydrated $K_2La_2Ti_3O_{10}\cdot 1.6H_2O$ adopting the *P*4/*mmm* tetragonal structure (ICDD card no. 01-087-11-68).

It should be mentioned, that in order to test the reliability of the optimized methodology, the synthesis was repeated several times and, in some cases, formation of a slightly amorphous phase could be observed.

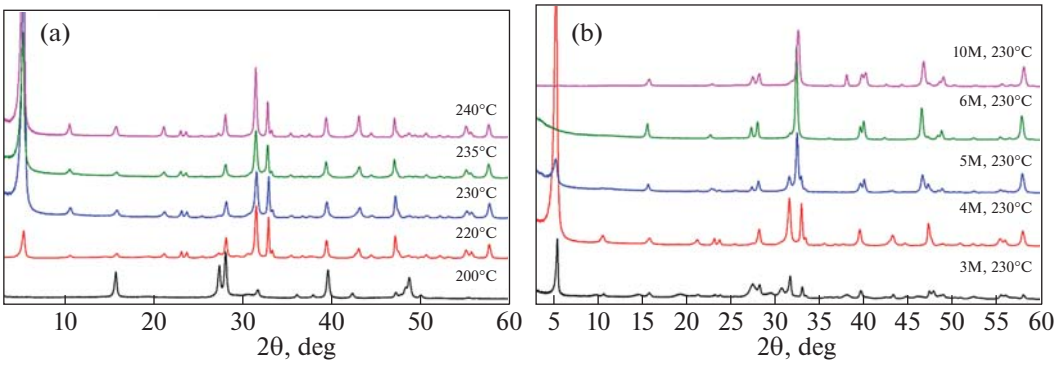

Fig. 2. XRD patterns of the samples obtained at varied temperatures (A) and varied concentrations of KOH solutions (B).

The crystallinity of the samples obtained at similar reaction conditions varied, however in all cases only single layered phase was observed. As the crystallization appeared to be highly sensitive to reaction conditions, we performed additional series of experiments in order to determine the borders of various conditions to obtain the layered phase successfully.

Figure 2A shows XRD patterns for the samples obtained at the temperature range of 220–240°C (4 M KOH, 72 h). As may be seen, in all the cases the formation of $K_2La_2Ti_3O_{10}$ is observed, however, an additional amorphous phase is also detected at 220°C. As shown earlier, heating at lower temperatures (200°C) does not lead to the formation of the layered phase. Higher temperatures were not tested due to the limits of thermal stability of Teflon-lined vessels used for the reaction.

The impact of KOH concentration on $K_2La_2Ti_3O_{10}$ formation was further studied.

Figure 2B shows XRD patterns for the samples obtained at 230–240°C heating for 72 h with various KOH solutions. Formation of the layered structure starts when we use 3 M KOH, however the sample is low crystalline and contains an amorphous secondary phase. The well-crystallized aimed phase is observed when using 4 M KOH and the further increase in the alkali concentration leads to the decrease of the layered compound yield and formation of a new phase $La_{0.5}K_{0.5}TiO_3$, which is obtained in a pure form using 6 and 10 M alkali.

In order to examine the impact of precursor's saturation in the medium during the reaction on the crystal growth, the series of experiments with various amount of precursors (stoichiometric amounts of TiO_2 and La_2O_3 calculated for 125, 250 and 500 mg of the aimed product) in a fixed volume of KOH solution has been performed. In all cases, the aimed layered phase could be successfully obtained with a slight impurity of an amorphous phase, so it may be concluded that the precursor's concentration does not have any significant impact on the synthesis.

3.2. Morphology

The morphology and particle sizes of the prepared ceramics were studied by scanning electron microscopy. SEM images for the samples obtained by the hydrothermal procedure in comparison with ones, prepared by the conventional high temperature synthesis, are shown in Fig. 3.

The particles in the sample obtained by the hydrothermal synthesis show a well-defined plate-like morphology with ~4–5 nm thickness (Fig. 3A) and relatively big lateral sizes of about 2–5 μm (Fig. 3B), unlike samples, obtained by the ceramic procedure (Figs. 3C, 3D). If we turn to the previously reported results, the lateral sizes of the particles obtained by the hydrothermal method were smaller than by the ceramic method, however no significant difference in thickness and morphology between ceramic and hydrothermal samples could be observed in SEM images presented in [28].

The impact of particles sizes and morphology on specific surface area was further tested by BET. The results for ceramic and hydrothermal samples are presented in Table 1. As may be seen from the table, employing the hydrothermal procedure leads to a significant increase in the specific surface area of the obtained powders.

3.3. Light Absorption and Photocatalytic Activity

Light absorption characteristics of the samples, obtained by the both methods, were studied by diffuse reflectance spectroscopy (DRS). Corresponding Tauc plots and calculated bandgap energies of the samples are presented in Fig. 4. As may be seen, the preparation procedure does not significantly affect the light absorption region although the hydrothermally obtained sample shows a slightly narrower band gap.

Kinetic curves of photocatalytic hydrogen generation over the studied samples (Fig. 5) demonstrate a predominantly linear dependence of the hydrogen amount in the system on time, i.e. the photocatalytic reaction rate in each case stays almost constant

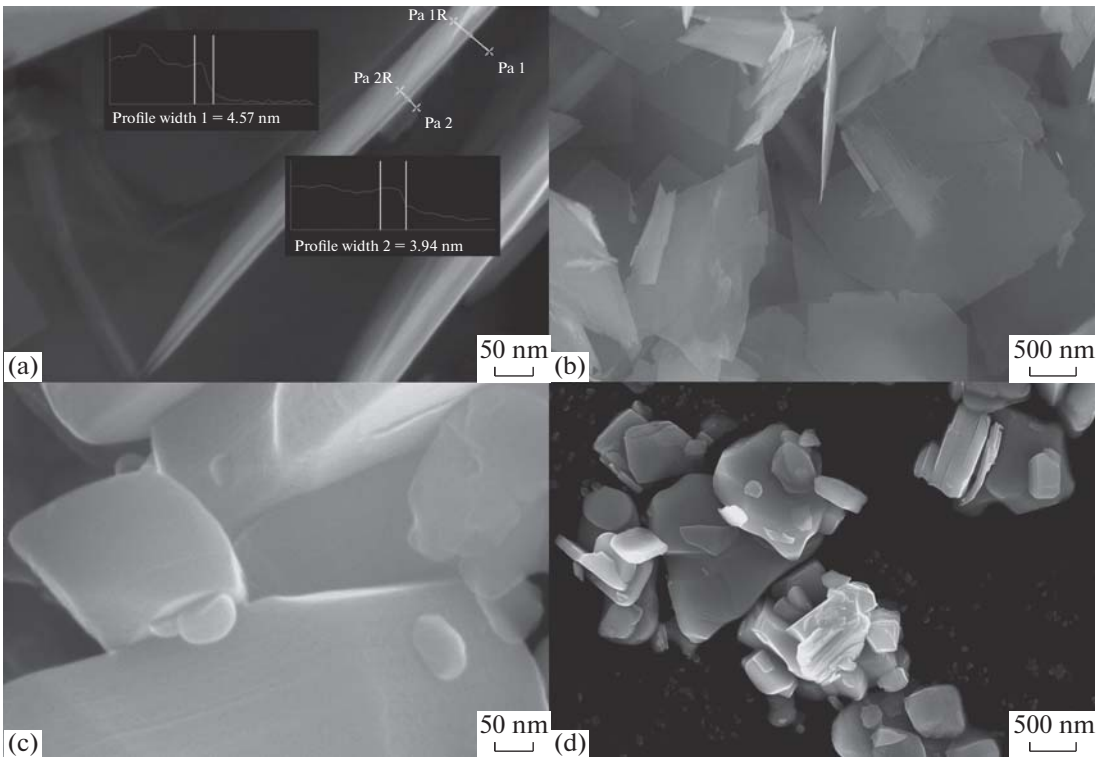

Fig. 3. SEM images of samples obtained by hydrothermal (A, B) and ceramic (C, D) methods.

throughout the measurement duration. Analysis of dark stages on the curves allows concluding that the reaction of aqueous methanol oxidation is indeed photocatalytic since the rate of hydrogen evolution gradually becomes zero after turning off the irradiation source.

Photocatalytic activity of the samples greatly depends on the preparation method. In particular, the hydrogen evolution rate over hydrothermally obtained bare $K_2La_2Ti_3O_{10}$ appears to be 2.5–3.5 times higher as compared with that of the ceramically synthesized analogue. This fact is quite expected due to larger specific surface area of the former, which cannot be achieved in the case of high temperature ceramic synthesis because of crystals intergrowth. Nevertheless, the ratio of photocatalytic activity values demonstrated by hydrothermal and ceramic bare titanates (~3) is significantly smaller than the ratio of their specific surfaces (~12). In other words, specific activity (calculated per unit surface area) of the former is ~4 times lower despite the larger surface. This feature may be associated with a lower degree of crystallinity of hydrothermal samples, and greater effect of surface electron-hole recombination. At the same time, the differences in photocatalytic activity of hydrothermal and ceramic $K_2La_2Ti_3O_{10}$ are not connected with the light absorption range since both samples have almost equal bandgap energies E_g.

In the presence of Pt as a cocatalyst, ceramically synthesized $K_2La_2Ti_3O_{10}$ shows the highest photocatalytic activity exceeding that of Pt-loaded hydrothermal samples by 4.6 times (Table 1). One of possible reasons for this fact is associated with the form of the titanate existence in the reaction medium. As was shown earlier, the alkaline phase $K_2La_2Ti_3O_{10}$ is not

Table 1. Photocatalytic activity of the products and auxiliary data

Sample	ω, μmol/h	φ, %	k_{Pt}	S, m^2/g		E_g, eV	λ_{max}, nm	c_1, mg/L	c_2, mg/L	c_3, mg/L	pH_1	pH_2	pH_3
				N_2	Kr								
Ceramic	5.4	0.0723	211	1.8	1.7	3.63	342	152	35.9	1.5	9.8	9.9	9.9
Ceramic /Pt	1140	15.2		—	—			150	150	0.4	8.9	6.8	6.8
Hydrothermal	14.1	0.189	17.5	20	21	3.56	348	449	424	1.4	9.5	7.5	7.5
Hydrothermal/Pt	247	3.30		—	—			492	347	0.3	7.8	7.1	7.2

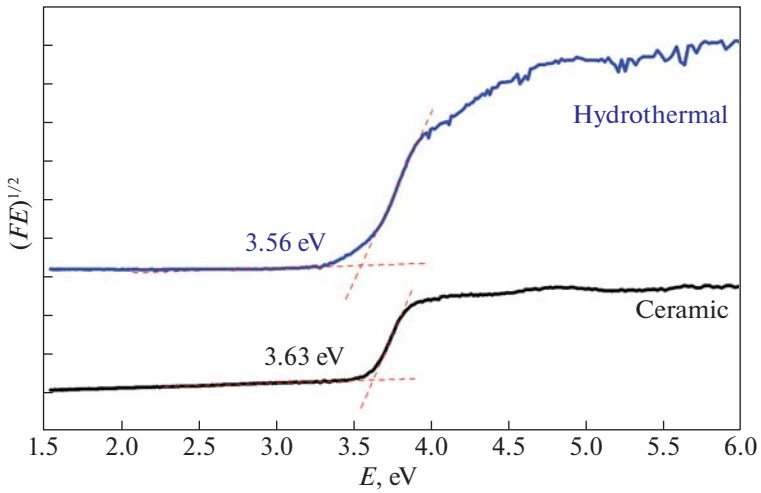

Fig. 4. Tauc plots for $K_2La_2Ti_3O_{10}$, obtained by hydrothermal and ceramic methods.

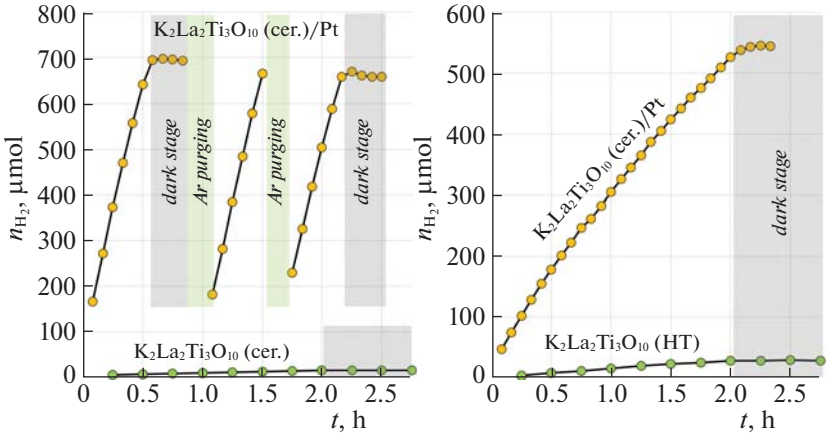

Fig. 5. Kinetic curves of photocatalytic hydrogen evolution over studied samples.

stable in aqueous solutions. Upon contact with water, the titanate undergoes ion exchange and water intercalation, giving partially protonated hydrated compounds $H_{2x}K_{2-2x}La_2Ti_3O_{10}{\cdot}yH_2O$, specific composition of which depends on pH of the medium [4]. As the pH value decreases, the protonation degree x increases and photocatalytic activity in the reaction of hydrogen generation goes down. In particular, fully protonated titanates ($x = 1$) show significantly smaller activity as compared with partially protonated ones, which is reported to be due to the lower degree of hydration y of their interlayer spaces [4]. The results obtained (Table 1) indicate that initial pH values of suspensions of platinized ceramic and hydrothermal $K_2La_2Ti_3O_{10}$ are different. The latter has more acidic medium, which should lead to the relatively greater degree of protonation x and, subsequently, lower activity. Moreover, the differences in morphology of ceramic and hydrothermal samples may affect completeness of Pt reduction and surface distribution of its nanoparticles, which requires more detailed studies.

Actual volume concentrations of the samples in photocatalytic suspensions (Table 1) also depend on their preparation methods. Whilst ceramically synthesized $K_2La_2Ti_3O_{10}$ due to bigger particles sizes precipitates largely on the reaction cell walls despite intensive stirring, its analogue obtained hydrothermally forms suspensions with much higher sedimentation stability. Consequently, the latter is more preferable in terms of practical use. Extremely low concentrations of the form exfoliated into nanolayers (c_3) observed in all cases point to the absence of the samples' lamination during photocatalytic experiments.

4. CONCLUSIONS

Hydrothermal synthesis using commercially available precursors has been developed for reproducible

preparation of perovskite-like oxide $K_2La_2Ti_3O_{10}$ ultrafine powders. Various conditions (temperature, time, alkali concentration, precursor's concentration) have been tested to obtain pure-phase well-crystalline product. The optimized reaction conditions are as follows: 4 M KOH alkali solution with TiO_2 (Evonik Aeroxide P25) and La_2O_3 mixture taken in stoichiometric amounts and heated at 230–240°C for 72 h. Lower temperatures are not sufficient for the successful reaction between precursors and the $La(OH)_3$ phase inevitably forms. Higher KOH concentrations lead to the formation of non-layered 3D perovskite $La_{0.5}K_{0.5}TiO_3$ and lower KOH concentration leads to the low-crystallized product. The obtained powders represent nanoplatelets with μm lateral sizes and 4–5 nm thickness, possessing enhanced specific surface area comparing to the ceramically obtained samples. Hydrothermally obtained bare $K_2La_2Ti_3O_{10}$ shows higher photocatalytic activity towards hydrogen evolution comparing to the ceramically obtained samples, however using Pt as a co-catalyst leads to the higher performance of the ceramically obtained powders, which may be the result of higher protonation of hydrothermally obtained sample during the photocatalytic process. Developed synthetic approach may be later applied for preparation of inorganic-organic hybrids and monolayers based on the $K_2La_2Ti_3O_{10}$ oxide, for further improvements of catalytic activity. Due to their ultrafine platelet-like morphology, obtained nanopowders may be also employed for composites preparation, as was shown in our previous work, where hydrothermally prepared $K_2La_2Ti_3O_{10}$ was used as a Torlon® polyamide-imide (PAI) membrane modifier [31].

ACKNOWLEDGMENTS

The study was conducted using the equipment of the Saint Petersburg State University Research Park: Centre for X-ray Diffraction Studies, Centre for Chemical Analysis and Materials Research, Interdisciplinary Centre for Nanotechnology, Centre for Thermal Analysis and Calorimetry, Centre for Innovative Technologies of Composite Nanomaterials.

FUNDING

This research was funded by the Russian Science Foundation (projects no. 19-13-00184).

CONFLICT OF INTEREST

The authors declare that they have no conflicts of interest.

REFERENCES

1. T. Takata, Y. Furumi, K. Shinohara, et al., Chem. Mater. **9**, 1063 (1997).
2. I. Rodionov and I. Zvereva, Russ. Chem. Rev. **85**, 248 (2016).
3. I. Rodionov, O. Silyukov, T. Utkina, et al., Russ. J. Gen. Chem. **82**, 1191 (2012).
4. I. Rodionov, E. Mechtaeva, A. Burovikhina, et al., Monatsh. Chem. **149**, 475 (2018).
5. W. Cui, L. Liu, S. Ma, Y. Liang, and Z. Zhang, Catal. Today **207**, 44 (2013).
6. D. Pang, J. Gao, F. Ouyang, et al., Catalysts **7**, 126 (2017).
7. I. Rodionov, E. Maksimova, A. Pozhidaev, et al., Front. Chem. **7**, 863 (2019).
8. S. Kurnosenko, V. Voytovich, O. Silyukov, et al., Catalysts **11**, 1279 (2021).
9. V. Voytovich, S. Kurnosenko, O. Silyukov, et al., Front. Chem. **8**, 300 (2020).
10. V. Voytovich, S. Kurnosenko, O. Silyukov, et al., Catalysts **11**, 897 (2021).
11. Y. Ebina, K. Akatsuka, K. Fukuda, and T. Sasaki, Chem. Mater. **24**, 4201 (2012).
12. A. Shiguihara, M. Bizeto, and V. Constantino, Colloids Surf., A **295**, 123 (2007).
13. T. Ozawa, K. Fukuda, Y. Ebina, and T. Sasaki, Inorg. Chem. **52**, 415 (2013).
14. S. Ida, Y. Okamoto, M. Matsuka, et al., J. Am. Chem. Soc. **134**, 15773 (2012).
15. S. Ida, C. Ogata, M. Eguchi, et al., J. Am. Chem. Soc. **130**, 7052 (2008).
16. I. Minich, O. Silyukov, S. Kurnosenko, et al., Nanomaterials **11**, 2708 (2021).
17. T. Oshima, Y. Wang, D. Lu, et al., Nanoscale Adv. **1**, 189 (2019).
18. Y. Liu, Y. Zhou, C. Lv, et al., New J. Chem. **42**, 681 (2018).
19. M. Raciulete, F. Papa, C. Negrila, et al., Catalysts **10**, 637 (2020).
20. K. Kawashima, M. Hojamberdiev, S. Chen, et al., Mol. Catal. **432**, 250 (2017).
21. K. Soongprasit, D. Aht-Ong, V. Sricharoenchaikul, and D. Atong, Curr. Appl. Phys. **12**, S80 (2012).
22. A. Ansari, N. Ahmad, M. Alam, et al., Sci. Rep. **9**, 1 (2019).
23. J. Dąbrowa, A. Olszewska, A. Falkenstein, et al., J. Mater. Chem. A **8**, 24455 (2020).
24. J. Lee, S. Bang, and W. Lee, Front. Chem. **10**, 873758 (2022).
25. W. Chen, C. Wang, P. Chen, et al., Catalysts **11**, 854 (2021).
26. H. Shen, T. Xue, Y. Wang, et al., Mater. Res. Bull. **84**, 15 (2016).
27. A. Yapryntsev, A. Baranchikov, and V. Ivanov, Russ. Chem. Rev. **89**, 629 (2020).
28. Y. Huang, J. Wu, Y. Wei, J. Lin, and M. Huang, J. Alloys Compd. **456**, 364 (2008).
29. M. Sakaki, R. Okubi, Y. Feng, and K. Kajiyoshi, Solid State Sci. **82**, 59 (2018).
30. K. Toda, J. Watanabe, and M. Sato, Mater. Res. Bull. **31**, 1427 (1996).
31. A. Pulyalina, V. Rostovtseva, I. Minich, et al., Symmetry **12**, 1142 (2020).

SPELL: 1. benchtop